Electronic Supplementary Material (ESI) for Materials Chemistry Frontiers.

Supporting Information

Simultaneously Excited Downshifting/Upconversion Luminescence from Lanthanide-Doped Core-Shell Lead-Free Perovskite Nanocrystals for Encryption and Data Storage

Endian Cui,[b1] Gaoyuan Xing,[b1] Xiangyang Yuan,[b] Yi Zhang,[b] Flavia Artizzu,[e] Xiaoling Liao,[b] Jianfeng Tang,[b] Yanan Zhao,[c] Pengzhou Zhao,[a] Kai Liu,*[d] Jing Liu*[a]

a. Department of Oncology, The People's Hospital of JiangMen, Jiangmen, 529000, China

b. Key Laboratory of Luminescence Analysis and Molecular Sensing, Ministry of Education, School of Materials and Energy, Southwest University, Chongqing, 400715, PR China

c. Analytical and Testing Center, Southwest University, Chongqing, 400715, PR China

d. College of Materials Science and Engineering, Chongqing Jiaotong University, Chongqing 400074, China

e. Department of Sustainable Development and Ecological Transition (DISSTE), University of Eastern Piedmont "A. Avogadro", Piazza S. Eusebio 5, 13100, Vercelli, Italy

* Corresponding authors.
E-mail: kai.liu@cqjtu.edu.cn; jingliu77@swu.edu.cn
[1] Endian Cui and Gaoyuan Xing contributed equally.

Table of contents

Section S1. Optical properties of undoped, Bi^{3+} doped and Yb^{3+}, Er^{3+} co-doped $Cs_2AgInCl_6$ NCs

As seen in Figure S5, the pristine $Cs_2AgInCl_6$ NCs are characterized by a strong PL excitation (PLE) peak at around 360 nm, due to surface-related sub-band gap states or defects,[1] which is related to a broad PL band peaked at 550 nm corresponding to white light emission. As can be seen from Figure S5b, $Cs_2AgInCl_6$ NCs have a strong absorbance under shorter wavelength irradiation (< 350 nm), and the direct band-gap value is 4.34 eV according to the Tauc plot (Figure S6a).

As seen Figure S7a, the incorporation of Bi^{3+} in $Cs_2AgInCl_6$ NCs significantly changes the optical absorption and the broadband visible emission. Under 370 nm excitation, the $Cs_2AgInCl_6$:Bi NCs exhibit a broad orange emission band at around 635 nm. This broadband STEs emission may derive from the large exciton binding energy caused by the Jahn-Teller distortion of the linked $AgCl_6$-$BiCl_6$ octahedron.[2] As the doping concentration is increased, the PL intensity reaches a maximum at 2% of Bi^{3+} (PLQY = 4.2%), then subsequently declines as a result of concentration quenching. In addition, the spectra show distinct red-shifted emission and excitation, which may be due to the variation in the edge structure of $Cs_2AgInCl_6$ NCs via Bi^{3+}

doping.[3] The red-shift in the emission of $Cs_2AgInCl_6$:Bi NCs can also be observed from the CIE diagram (Figure S7b and Table S3). Two broad excitation bands appear in the PLE spectra, which are centered at 320 nm and 370 nm (Figure S7a), in agreement with the absorption spectrum shown in Figure S5b. The excitation band at 320 nm corresponds to the sub-band gap shallow trap state, and the other band at 370 nm matches the spin-allowed $^1S_0 \rightarrow {}^3P_1$ transition of Bi^{3+}.[4] The bandgap value of 2%Bi NCs is indicated in Figure S6b, according to its Tauc plot. The incorporation of Bi^{3+} into $Cs_2AgInCl_6$ DP reshapes the band structure and leads to the characteristics of indirect band gap, due to the variation in the conduction band minimum.[4] We also performed PL decay measurements on $Cs_2AgInCl_6$ and 2%Bi NCs to illustrate the origins of the emission (Figure S7c and S7d). The retrieved average lifetimes (τ_{avg}) of $Cs_2AgInCl_6$ and 2%Bi NCs are 4.34 ns and 195.64 ns, respectively. Figure S7e shows the energy level diagram of Bi^{3+}, which can be excited from the $^1S_0$ level to $^1P_1$ level or ^3P_n level (n = 0, 1, 2). The possible PL mechanism of Bi^{3+} centers in the $Cs_2AgInCl_6$:Bi NCs is proposed in Figure 3c. Bi^{3+} can absorb 370 nm photons and is photoexcited to $^3P_1$ and $^1P_1$ levels, then the $^1P_1$ level relaxes to the $^3P_1$ level, subsequently transferring the energy to the STE state and leading to the observation of orange light emission.

Here, in order to broaden the excitation wavelength range of $Cs_2AgInCl_6$ NCs, we introduced Yb^{3+} and Er^{3+} into $Cs_2AgInCl_6$ NCs to achieve visible upconversion emission under NIR excitation and enrich the PL properties of DP. As seen from Figure S8a, under 980 nm excitation, Yb^{3+}-Er^{3+} co-doped $Cs_2AgInCl_6$ display

narrowband visible emission centered at 526 nm, 552 nm, and 665 nm, corresponding to $^2H_{11/2} \rightarrow {}^4I_{15/2}$, $^4S_{3/2} \rightarrow {}^4I_{15/2}$ and $^4F_{9/2} \rightarrow {}^4I_{15/2}$ transitions of Er^{3+}, respectively. The possible upconversion mechanism is illustrated in Figure S8d. Under 980 nm light, Yb^{3+}, which has a 10 times larger absorption cross-section than erbium, is first photoexcited from the $^2F_{7/2}$ to the $^2F_{5/2}$ level. Then the Er^{3+} $^4I_{11/2}$ energy level becomes populated by energy transfer favored by the energy match with the $^2F_{5/2}$ energy level of Yb^{3+}, while Yb^{3+} depopulates from the $^2F_{5/2}$ excited state to $^2F_{7/2}$ ground state. As the Er^{3+} $^4I_{11/2}$ level is relatively long-lived, further photoexcitation can lead to the population of the upper $^4F_{7/2}$ level, which will then relax to the lower energy levels $^2H_{11/2}$, $^4S_{3/2}$ and $^4F_{9/2}$. Eventually Er^{3+} will return to the ground state $^4I_{15/2}$ by radiative relaxation resulting in green and red emissions. With the increase of Er^{3+} doping concentration, the upconversion intensity of 20%Yb, 7%Er NCs reaches a maximum and subsequently decreases (Figure S8a and S8b). As the excitation wavelength is increased from 280 to 370 nm, the broadband STEs emission of the DP host, centered at around 590 nm is revealed via the PL spectra of 20%Yb, 7%Er NCs (Figure S9a). Compared with the pristine nanocrystals, the co-doped NCs exhibit red-shifted emission, which may be attributed to the lattice distortion caused by the doping of Yb^{3+} and Er^{3+}. In agreement, the band gap value of 20%Yb, 7%Er NCs as estimated from its Tauc plot (Figure S6c), is reduced to 4.24 eV.[5] The observed emission average lifetime is 4.45 ns, which is consistent with with the value measured for the undoped NCs (Figure S8c). When illuminated under 365 nm laser, white light is emitted from the Yb^{3+}-Er^{3+} co-doped NCs (Figure S9b).

Section S2. Supplementary Figures and Tables

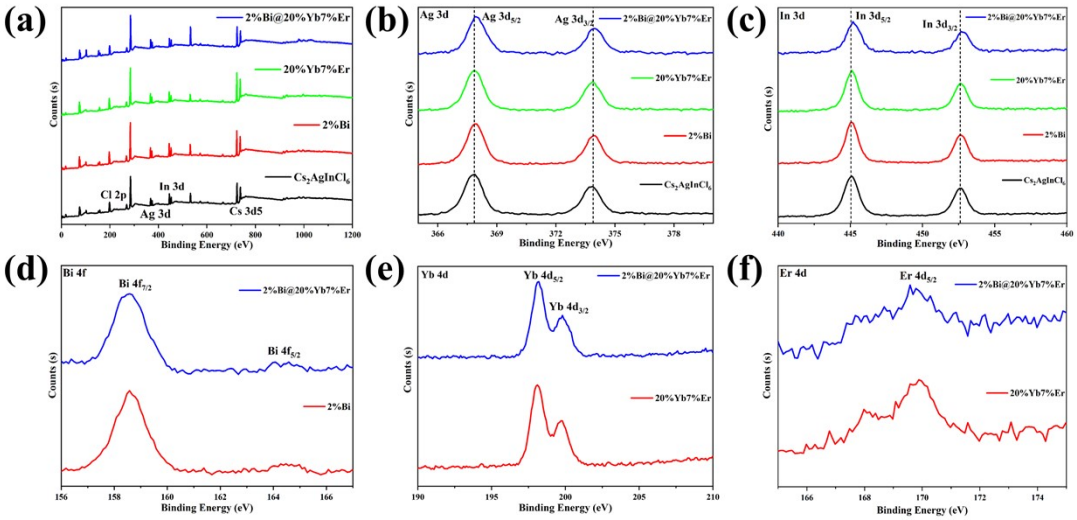

Figure S1. (a) Survey XPS spectra for $Cs_2AgInCl_6$, 2%Bi, 20%Yb, 7%Er, 2%Bi@20%Yb, 7%Er; High-resolution XPS spectra of (b) Ag 3d, (c) In 3d, (d) Bi 4f, (e) Yb 4d and (f) Er 4d, respectively.

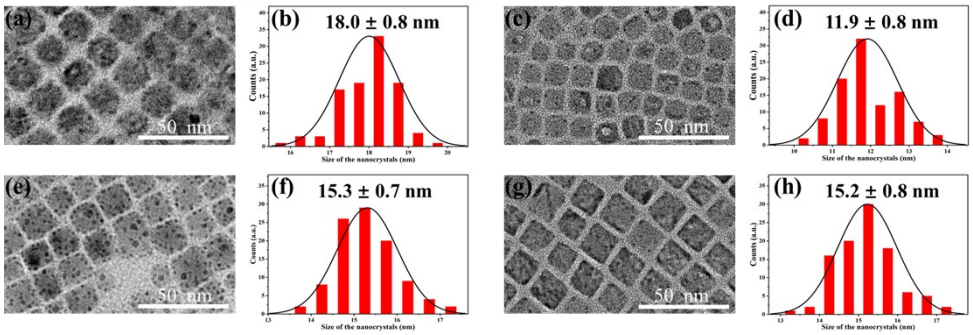

Figure S2. Size distribution estimated from TEM image of double perovskite nanocrystals. (a, b) $Cs_2AgInCl_6$; (c, d) 2%Bi; (e, f) 20%Yb, 7%Er; (g, h) 2%Bi@20%Yb, 7%Er.

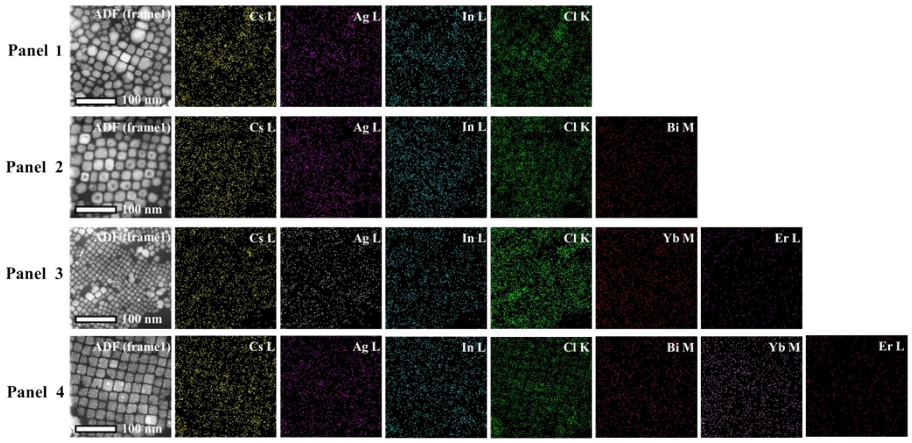

Figure S3. TEM-EDS mapping images. Panel 1: $Cs_2AgInCl_6$; Panel 2: 2%Bi; Panel 3:

20%Yb, 7%Er and Panel 4: 2%Bi@20%Yb, 7%Er.

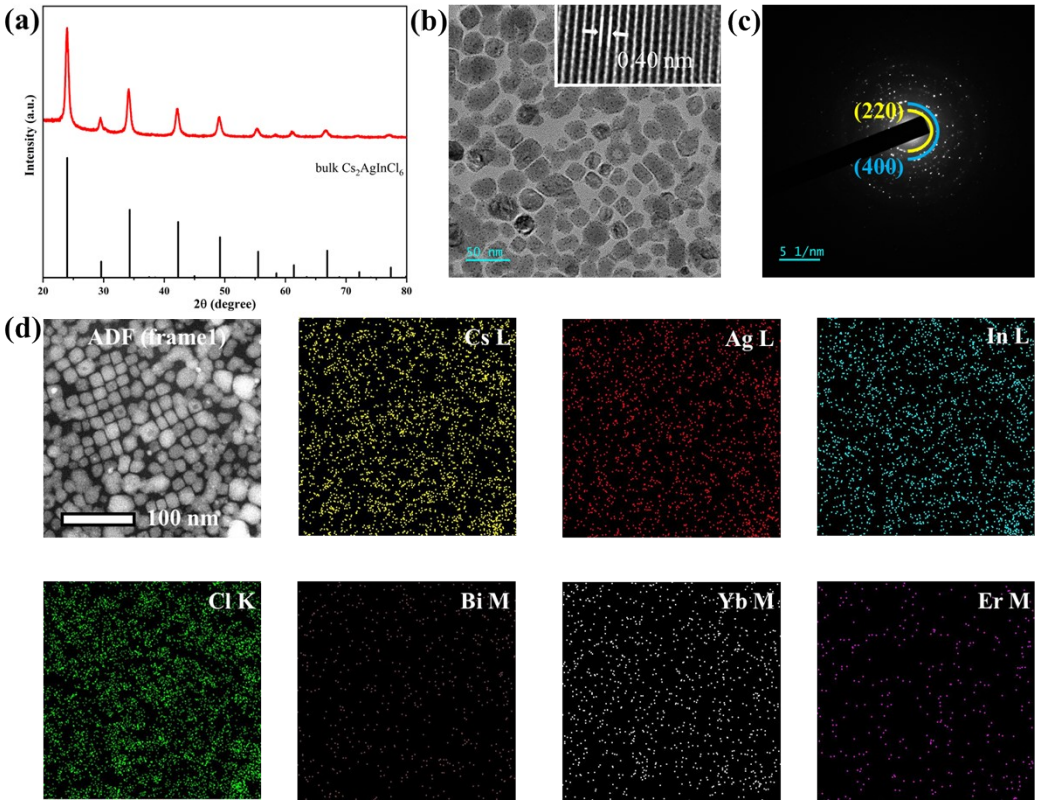

Figure S4. XRD pattern and TEM images of the mixture of 2%Bi and 20%Yb, 7%Er. (a) XRD pattern; (b) TEM and HRTEM images; (c) the corresponding SAED patterns; (d) TEM-EDS mapping images.

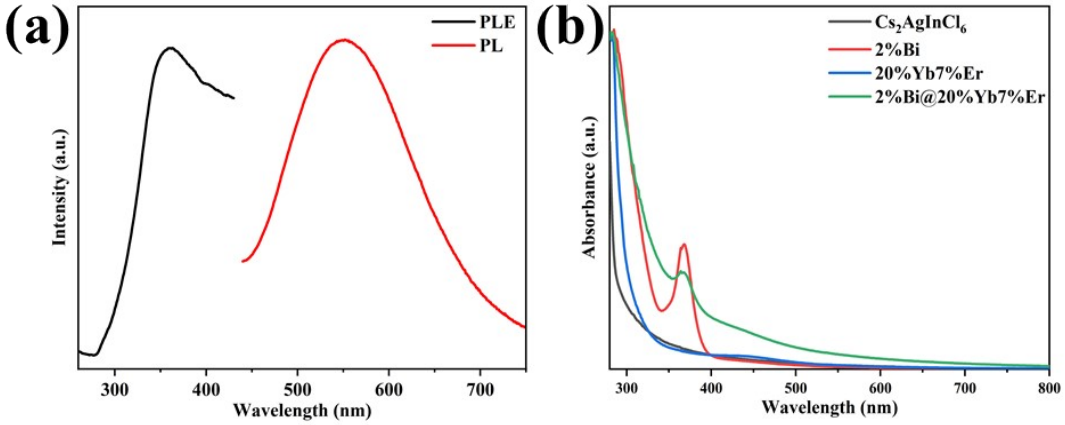

Figure S5. (a) PLE (λ_{em} = 550 nm) and PL (λ_{ex} = 360 nm) spectra of $Cs_2AgInCl_6$ NCs dispersed in cyclohexane; (b) UV−visible absorption spectra of $Cs_2AgInCl_6$, 2%Bi, 20%Yb, 7%Er, 2%Bi@20%Yb, 7%Er NCs dispersed in cyclohexane.

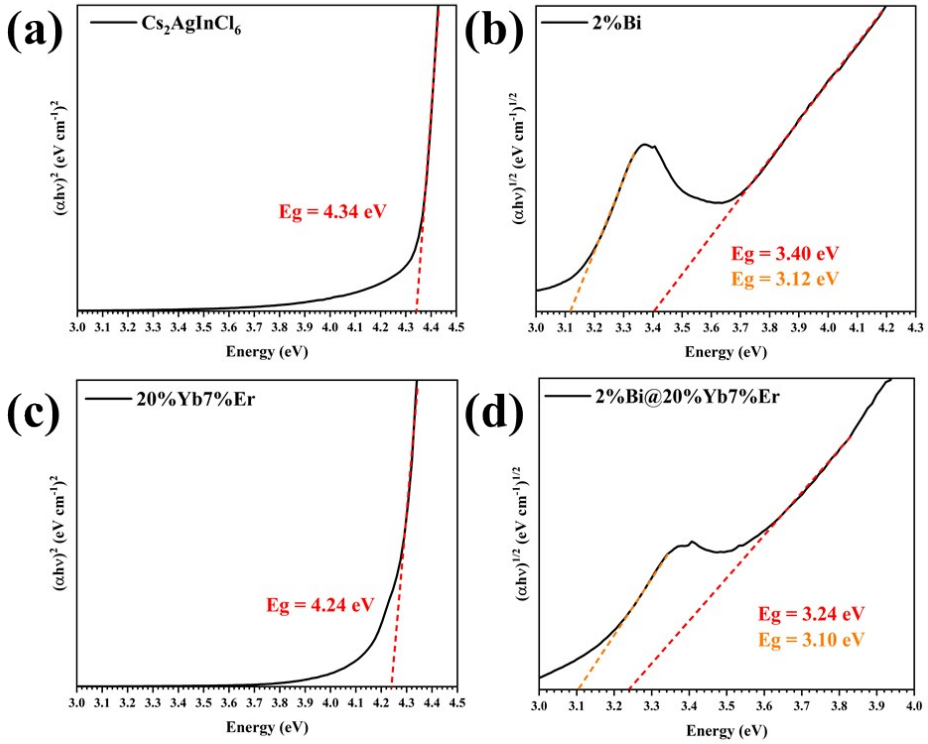

Figure S6. $(\alpha h\nu)^2$-hν plots of (a) $Cs_2AgInCl_6$, (b) 2%Bi, (c) 20%Yb, 7%Er, (d) 2%Bi@20%Yb, 7%Er NCs. The value of the optical band gap can be derived from the extrapolation to $\alpha = 0$.

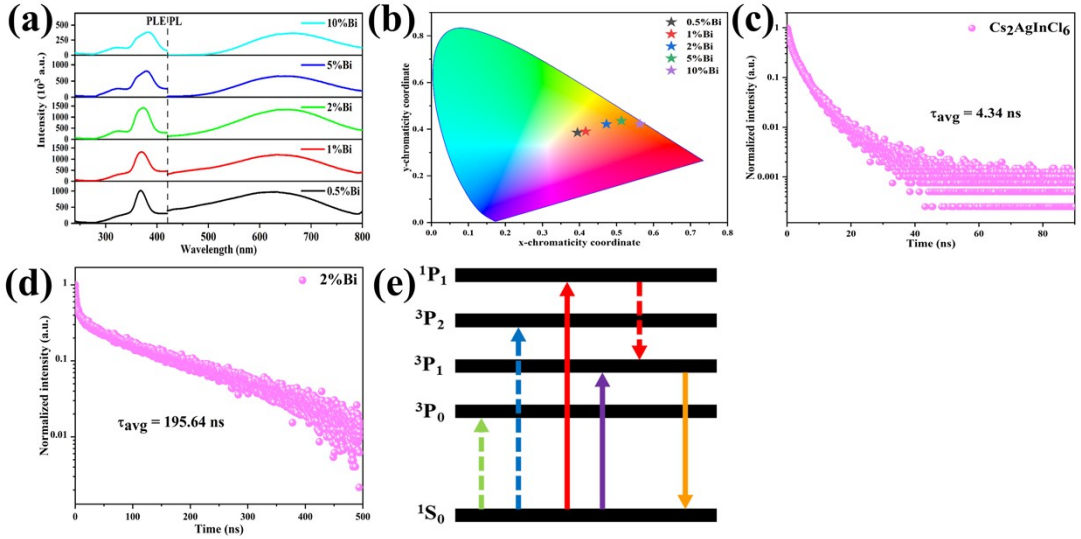

Figure S7. (a) PL (λ_{ex} = 370 nm) and PLE (λ_{em} = 635 nm) spectra of $Cs_2AgInCl_6$:x%Bi (x = 0.5, 1, 2, 5, 10); (b) the corresponding Commission International de I'Eclairage (CIE) coordinates diagram; (c) PL decay curve of $Cs_2AgInCl_6$ emission at 550 nm under 375 nm excitation; (d) PL decay curve of 2%Bi emission at 635 nm under 375 nm excitation; (e) energy level diagram of Bi^{3+}.

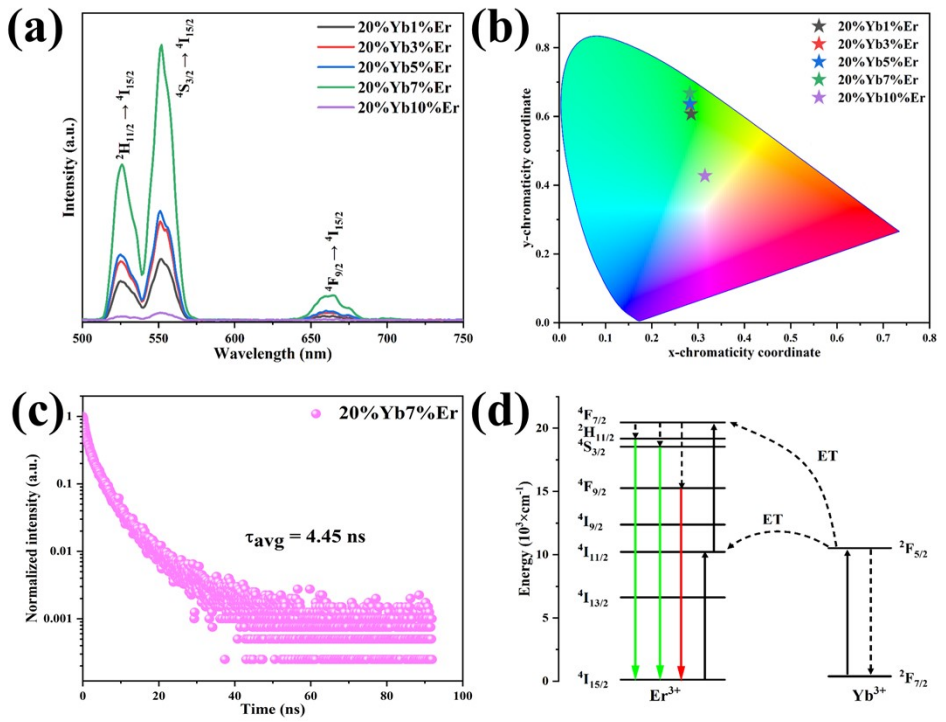

Figure S8. (a) PL (λ_{ex} = 980 nm) spectra of $Cs_2AgInCl_6$:20%Yb, y%Er (y = 1, 3, 5, 7, 10); (b) the corresponding CIE coordinates image; (c) PL decay curve of 20%Yb, 7%Er emission at 550 nm under 375 nm excitation; (d) schematic diagram of energy-transfer mechanism in $Cs_2AgInCl_6$:Yb, Er NCs.

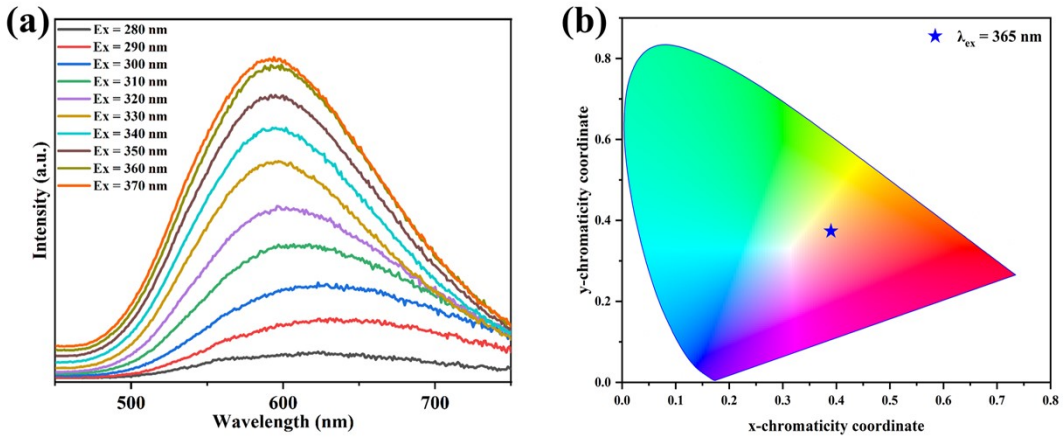

Figure S9. (a) the PL spectra of 20%Yb, 7%Er NCs excited at different wavelengths; (b) the CIE coordinates image of 20%Yb, 7%Er NCs under the excitation of 365 nm.

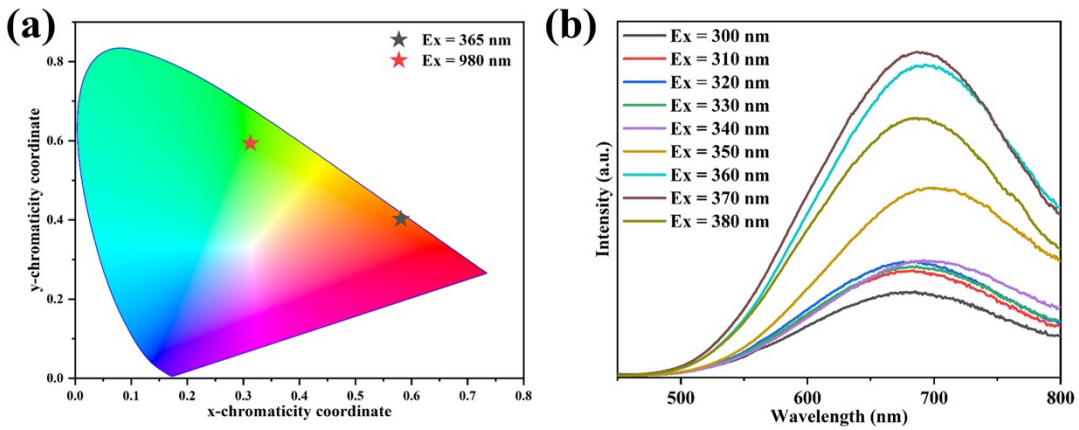

Figure S10. (a) CIE coordinates diagram for the emission under 365 nm and 980 nm illumination; (b) PL spectra of 2%Bi@20%Yb, 7%Er NCs at different excitation wavelengths. On increasing the excitation wavelength (Figure S10b), the broadband STEs emission centered at around 690 nm still dominates the spectrum while increasing in intensity, indicating that Bi^{3+}-induced emission does not shift compared to vis emission from the matrix.

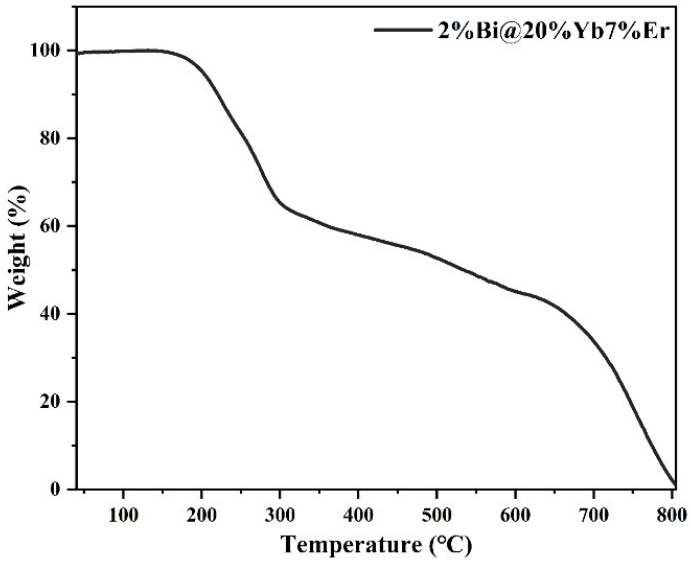

Figure S11. TG curve of 2%Bi@20%Yb, 7%Er NCs. TG measurement show that the weight loss at 300 °C is attributed to the evaporation of cyclohexane, DPE, OA, Olam[6] and the core-shell DP structure decomposes around 600 °C.

Table S1. Structural parameters estimated from XRD patterns.

	Space group	Cell parameters(Å)	Cell volume(Å^3)	R^2
$Cs_2AgInCl_6$	Fm-3m	a=10.474	1149.05	0.9590
2%Bi	Fm-3m	a=10.477	1150.03	0.9766
20%Yb, 7%Er	Fm-3m	a=10.518	1163.59	0.9292
2%Bi@20%Yb, 7%Er	Fm-3m	a=10.509	1160.60	0.9361

Table S2. ICP elemental analysis of $Cs_2AgInCl_6$, $Cs_2AgInCl_6$:2%Bi, $Cs_2AgInCl_6$:20%Yb, 7%Er, $Cs_2AgInCl_6$:2%Bi@$Cs_2AgInCl_6$:20%Yb, 7%Er NCs.

	Content ratio (Cs:In)	Content ratio (Bi:In)	Content ratio (Yb:In)	Content ratio (Er:In)
$Cs_2AgInCl_6$	2.15	0	0	0
2%Bi	2.25	0.03	0	0
20%Yb, 7%Er	2.47	0	0.19	0.07
2%Bi@20%Yb, 7%Er	2.43	0.02	0.05	0.02

Table S3. CIE coordinates of $Cs_2AgInCl_6$:x%Bi NCs (x = 0.5, 1, 2, 5, 10).

	0.5%Bi	1%Bi	2%Bi	5%Bi	10%Bi
X	0.39	0.42	0.47	0.51	0.56
Y	0.39	0.39	0.42	0.44	0.42

Section S3. Supplementary References

1. Y. Liu, Y. Jing, J. Zhao, Q. Liu and Z. Xia, Design optimization of lead-free perovskite $Cs_2AgInCl_6$:Bi nanocrystals with 11.4% photoluminescence quantum yield, Chem. Mater., 2019, **31,** 3333-3339.
2. Y. Pei, D. Tu, C. Li, S. Han, Z. Xie, F. Wen, L. Wang and X. Chen, Boosting near-infrared luminescence of lanthanide in $Cs_2AgBiCl_6$ double perovskites via breakdown of the local site symmetry, Angew. Chem. Int. Ed., 2022, **61**, e202205276.
3. S. Jin, R. Li, H. Huang, N. Jiang, J. Lin, S. Wang, Y. Zheng, X. Chen and D.

Chen, Compact ultrabroadband light-emitting diodes based on lanthanide-doped lead-free double perovskites, Light Sci. Appl., 2022, **11**, 52.

4. D. Manna, T.K. Das and A. Yella, Tunable and stable white light emission in Bi^{3+}-alloyed $Cs_2AgInCl_6$ double perovskite nanocrystals, Chem. Mater., 2019, **31**, 10063-10070.
5. Z. Rao, Q. Li, Z. Li, L. Zhou, X. Zhao and X. Gong, Ultra-high-sensitive temperature sensing based on Er^{3+} and Yb^{3+} co-doped lead-free double perovskite microcrystals, J. Phys. Chem. Lett, 2022, **13**, 3623-3630.
6. F. Locardi, M. Cirignano, D. Baranov, Z. Dang, M. Prato, F. Drago, M. Ferretti, V. Pinchetti, M. Fanciulli, S. Brovelli, L. De Trizio and L. Manna, Colloidal synthesis of double perovskite $Cs_2AgInCl_6$ and Mn-doped $Cs_2AgInCl_6$ nanocrystals, J. Am. Chem. Soc., 2018, **140**, 12989-12995.